Green Bank and Effelsberg Radio Telescope Searches for Axion Dark Matter Conversion in Neutron Star Magnetospheres

Foster, J.W.; Kahn, Y.; Maclas, O.; Sun, Z.; Eatough, R.P.; Kondratiev, V.I.; Peters, W.M.; Weniger, C.; Safdi, B.R.

DOI
10.1103/PhysRevLett.125.171301

Publication date
2020

Document Version
Final published version

Published in
Physical Review Letters

Featured in Physics

Green Bank and Effelsberg Radio Telescope Searches for Axion Dark Matter Conversion in Neutron Star Magnetospheres

Joshua W. Foster,[1,*] Yonatan Kahn,[2] Oscar Macias,[3,4] Zhiquan Sun,[1] Ralph P. Eatough,[5,6] Vladislav I. Kondratiev,[7,8] Wendy M. Peters,[9] Christoph Weniger,[4,†] and Benjamin R. Safdi[1,‡]

[1]*Leinweber Center for Theoretical Physics, Department of Physics, University of Michigan, Ann Arbor, Michigan 48109, USA*
[2]*University of Illinois at Urbana-Champaign, Urbana, Illinois 61801, USA*
[3]*Kavli Institute for the Physics and Mathematics of the Universe (WPI), University of Tokyo, Kashiwa, Chiba 277-8583, Japan*
[4]*GRAPPA Institute, Institute of Physics, University of Amsterdam, 1098 XH Amsterdam, Netherlands*
[5]*National Astronomical Observatories, Chinese Academy of Sciences, 20A Datun Road, Chaoyang District, Beijing 100101, People's Republic of China*
[6]*Max-Planck-Institut fur Radioastronomie, Auf dem Hugel 69, D-53121 Bonn, Germany*
[7]*ASTRON, the Netherlands Institute for Radio Astronomy, Oude Hoogeveensedijk 4, 7991 PD Dwingeloo, Netherlands*
[8]*Astro Space Centre, Lebedev Physical Institute, Russian Academy of Sciences, Profsoyuznaya Street 84/32, Moscow 117997, Russia*
[9]*Naval Research Laboratory, Remote Sensing Division, Code 7213, Washington, DC 20375-5320, USA*

(Received 14 May 2020; revised 26 July 2020; accepted 17 September 2020; published 20 October 2020)

Axion dark matter (DM) may convert to radio-frequency electromagnetic radiation in the strong magnetic fields around neutron stars. The radio signature of such a process would be an ultranarrow spectral peak at a frequency determined by the mass of the axion particle. We analyze data we collected from the Robert C. Byrd Green Bank Telescope in the *L* band and the Effelsberg 100-m Telescope in the *L* band and *S* band from a number of sources expected to produce bright signals of axion-photon conversion, including the Galactic center of the Milky Way and the nearby isolated neutron stars RX J0720.4-3125 and RX J0806.4-4123. We find no evidence for axion DM and are able to set constraints on the existence of axion DM in the highly motivated mass range between ∼5 and 11 μeV with the strongest constraints to date on axions in the ∼10–11 μeV range.

DOI: 10.1103/PhysRevLett.125.171301

Recently, it was proposed that radio telescope observations of neutron stars (NSs) can probe axion dark matter (DM) [1–5]. In the magnetosphere surrounding a NS, axion DM may resonantly convert into radio-frequency photons at locations where the plasma frequency of the magnetosphere equals the axion mass, with conversion probabilities determined in part by the strength of the magnetic field surrounding the NS. The central frequency of the hypothetical radio signal from an individual NS is set by the mass of the axion, redshifted by the line-of-sight velocity of the NS. The predicted axion-induced radio signal would appear as a nearly monochromatic peak in the otherwise smoothly varying radio spectrum from the NS and its nearby environment. The frequency of this peak is universal for all sources and is determined by the currently unknown mass of the axion particle.

In Refs. [3–6], it was shown that high-frequency-resolution observations with radio telescopes such as the Robert C. Byrd Green Bank Telescope (GBT) and the Effelsberg 100-m Telescope toward nearby isolated NSs (INSs) and toward regions of high NS and DM density, such as the Galactic center (GC) of the Milky Way, would be sensitive to vast regions of previously unexplored axion parameter space. In this work, we perform such searches with the GBT and the Effelsberg radio telescope.

The quantum chromodynamics (QCD) axion is a well-motivated DM candidate, because, in addition to explaining the observed abundance of DM [7–9], it may also resolve the strong CP problem of the neutron electron dipole moment [10–13] (see [14] for a detailed review). The QCD axion may make up the observed abundance of DM over a wide range of masses [15], but a natural mass range is 5–25 μeV. In this work, we target axion masses in the range $m_a \in (4.5, 10.5)$ μeV, corresponding to radio frequencies $f = m_a/(2\pi) \in (1.1, 2.7)$ GHz.

The conversion of axion DM to radio photons arises from the Lagrangian $\mathcal{L} = g_{a\gamma\gamma} a \mathbf{E} \cdot \mathbf{B}$, where $\mathbf{E}$ ($\mathbf{B}$) are electric (magnetic) fields, a is the axion field, and $g_{a\gamma\gamma}$ is a coupling constant with units of inverse energy. For the QCD axion, $g_{a\gamma\gamma}$ is proportional to m_a, but models of more general axionlike particles can have $g_{a\gamma\gamma}$ and m_a as independent parameters. The mass range that we target here with radio telescope searches is also the subject of significant long-standing laboratory search efforts for the coupling $g_{a\gamma\gamma}$. The Rochester-Brookhaven-Fermilab (RBF) [16,17] and University of Florida (UF) [18] axion haloscope experiments set competitive constraints on axion DM in the mass range covered by this analysis, though our results exclude new parameter space beyond what was probed by those experiments. More recently, the ADMX

TABLE I. The targets observed by the GBT and Effelsberg for evidence of axion DM. "Pop." refers to populations of NSs, while "INS" refers to a single isolated NS. The bin widths $\delta f_{\rm obs}$ correspond to those of the original observation, but we down-bin the data before performing the axion line search to the resolution given by $\delta f_{\rm fid}$ to account for the finite width of the signal. The INS (GC) observations were performed with the GBT (Effelsberg radio telescope). The GBT INS observations cover the frequency range 1.15–1.73 GHz, with a gap from 1.2 to 1.35 GHz, and the L-band (S-band) Effelsberg observation covers 1.27–1.45 GHz (2.4–2.7 GHz). Note that the $t_{\rm exp}$ are the on exposure times.

Target	$t_{\rm exp}$ [min]	$\delta f_{\rm obs}$ [kHz]	$\delta f_{\rm fid}$ [kHz]	Type
RX J0806.4-4123	20.0	0.8	8.4	INS
RX J0720.4-3125	20.0	0.8	8.4	INS
GC (Eff., S band)	61.9	3.81	11.44	Pop.
GC (Eff., L band)	40.0	2.44	7.32	Pop.

experiment has reached sensitivity to the QCD axion at ∼2–3.5 μeV [19–21], and the haloscope at yale sensitive to axion CDM experiment has set strong constraints on axion DM in the mass range $m_a \sim 23$–24 μeV [22].

Data acquisition.—We collected data in the L band (1.15–1.73 GHz) with the GBT and in the L band (1.27–1.45 GHz) and S band (2.4–2.7 GHz) using the Effelsberg radio telescope to search for axion DM signatures from a variety of different sources. We describe the data taking procedures from the two telescopes in turn.

GBT observations.—The GBT observations were performed with the Versatile GBT Astronomical Spectrometer (VEGAS) backend [23] on March 10 and 29, 2019, with a notch filter applied from 1.2 to 1.34 GHz, so these frequencies are not included in our analysis (project AGBT19A_362, PI: Safdi). The nearby INS targets observed by the GBT are summarized in Table I. Note that we also observed the GC, M31, and M54 with the GBT, but the resulting axion limits are less robust than those from the INSs and from the Effelsberg GC observations and so are presented in Supplemental Material [24]. (The GBT GC observations lead to weaker limits than the Effelsberg GC observations, because the GBT observations were taken with lower frequency resolution.) All observations used the "spectral line" observing type and with one beam covering an area on the sky $\sim\pi(\mathrm{FWHM}/2)^2$, where FWHM is the full width at half maximum of the telescope response, which is 8.4′ at 1.5 GHz for the GBT.

The INS observations used five VEGAS spectrometers in mode 9 across the L band, leading to the frequency resolution $\delta f_{\rm obs}$ reported in Table I. For our fiducial analyses, the data are further down-binned to resolutions $\delta f_{\rm fid}$ given in Table I. Data were collected in both polarizations, though in this analysis we analyze only the polarization-averaged flux. (See [3] for possible polarization signatures.) The observations performed position switching so that, for a given observational target, half the data collection time was on source ("on") and half was spent observing blank-sky locations at similar elevations ("off") in order to establish a reference baseline for the analysis. The on exposure times $t_{\rm exp}$ are listed in Table I. The off locations were chosen to be 1.25° away from the target of interest. The position switching was carried out at 5-min intervals for each of the targets, leading to four separate observations of on and off positions.

Over the observing period, data were saved in independent short exposures for on and off observations of RX J0720.4-3125 and RX J0806.4-4123. In each successive exposure, a calibration noise diode was alternated between on and off with a switching period of 0.2097 s. The timing resolution allows for the identification of transient effects and data filtering, which is discussed further below and in Supplemental Material [24]. The calibration source 3C48 was observed for approximately 2 min to flux-calibrate the INS observations. Additionally, we observed the star-forming region W3(OH) for approximately 5 min to verify that our analysis framework is able to successfully identify the OH maser lines.

Effelsberg observations.—We also carried out L-band and S-band observations with the Effelsberg 100-m radio telescope toward the GC (project 77-17, 64-18, PI: Desvignes). The observations were taken with the PSRIX backend [36]—performing baseband sampling—in mid-June 2018 and early February 2019 using the prime (secondary) focus receiver P217 mm (S110 mm) for the L and S band, respectively. In both cases, we recorded orthogonal polarizations, which were later averaged offline for further analysis. Note that the FWHM of the Effelsberg beam is 9.78′ (4.58′) at 1.408 GHz (2.64 GHz). Observations were carried out toward the magnetar SGR J1745-2900, which is ∼2.4″ away from the GC, and the planetary nebula NGC7027 for subsequent use in the flux calibration procedure. For the measurements toward the GC, we used a position switching mode, with on-source integration times of 61.9 and 40.0 min for the S band and L band, respectively, and respective off-source integration times of 22.8 and 37.0 min (see Table I). The on observation was performed first, followed by a single off observation taken 16.4° away from the GC.

Analysis.—We reduced and calibrated the GBT data following a modified implementation of the GBTIDL data reduction pipeline [37], extended to include a time-series data filtering performed independently at each channel and a channel-dependent system temperature calibration. The full procedure results in measurements of flux densities $\{d_i\}$ at frequencies $\{f_i\}$, with i labeling the frequency channel. Because the stacked, calibrated data have been constructed by averaging many ($> 10^3$) independent antenna measurements together, the $\{d_i\}$ are approximately normally distributed.

For Effelsberg, high-resolution frequency spectra (131072 spectral channels) were generated from the raw

"baseband" data using the DSPSR [38] software tools [39]. We used the full-integrated spectra in our analysis, with a calibration procedure described in Supplemental Material [24]. Before analyzing the data, we first down-bin in frequency space to bins of width ∼8 kHz (see Table I) to account for the finite width of the signal, such that the majority of the signal should appear in a single frequency bin. As discussed further in Supplemental Material [24] and first suggested in Ref. [5], reflection and refraction of the outgoing electromagnetic waves in the rotating plasma induces a frequency broadening at the level $\delta f/f \sim 5 \times 10^{-6}$ or less from the INSs. We note that, even though the Effelsberg observations are searching for emission from a population of NSs, the data are at sufficiently high frequency resolution that we may search simply for the brightest converting NS from that population.

To inspect the data for excess flux at frequency channel i, we construct the likelihood

$$\mathcal{L}_i(\mathbf{d}|A,\mathbf{a}) = \prod_k \frac{1}{\sqrt{2\pi\sigma_k^2}} \exp\left[-\frac{[d_k - \mu(f_k|\mathbf{a}) - A\delta_{ik}]^2}{2\sigma_k^2}\right], \tag{1}$$

where A is the excess flux density in the central frequency channel. Note that the index k labels the analysis-level frequency channel, and the product runs over the frequency bins included in the analysis window. We model the background in the narrow sliding frequency window with a frequency-dependent mean flux density $\mu(f|\mathbf{a})$ and a single variance parameter σ^2, such that the variance in each frequency channel is given by $\sigma_i^2 = \sigma^2/\alpha_i$ for an acceptance fraction α_i of data at frequency channel i after the data filtering. Note that $\alpha_i = 1$ for all Effelsberg frequency channels, as we do not apply the time-filtering procedure to that data. The nuisance parameter vector $\mathbf{a}$ characterizes the frequency dependence of the mean; in practice, we take μ to be a quadratic function of f so that $\mathbf{a}$ has three independent parameters, though our final results are not sensitive to this choice (see Supplemental Material [24]).

In our fiducial analysis, we include within the sliding analysis window the ten frequency bins to the left and to the right of the central frequency channel, excluding the two bins on either side of the signal bin in case of signal leakage into those bins, if, e.g., the axion mass does not line up with the bin center. Note that to account for this possibility we also perform the analyses with all frequency bins shifted by approximately half a bin spacing. The variance parameter σ^2 is fixed by fitting the background-only model to the frequency sidebands with the central frequency channel masked out. We construct the profile likelihood $\mathcal{L}_i(\mathbf{d}|A)$ by maximizing $\mathcal{L}_i(\mathbf{d}|A,\mathbf{a})$ over the nuisance parameters $\mathbf{a}$ at each fixed value of A, and we use the profile likelihood to construct the one-sided 95% upper limit on the flux density as shown in Fig. 1 (see, e.g., [40]). In particular, we consider positive and negative values of A, and we take the 95% upper limit to be the value of $A > \hat{A}$ such that $2[\ln \mathcal{L}_i(\mathbf{d}|A) - \ln \mathcal{L}_i(\mathbf{d}|\hat{A})] \approx -2.71$, where $\hat{A}$ is the signal parameter that maximizes the profile likelihood. We then further power constrain our limits to avoid setting limits that are stronger than expected due to downward statistical fluctuations [41]. We accomplish this by recording the actual limit as the maximum of the 16th percentile of the distribution of expected limits under the null hypothesis, as computed using the Asimov procedure [40], and the limit observed on the actual data. Our test statistic (TS) for comparing signal and null hypotheses for evidence of an axion is the log-likelihood ratio $\mathrm{TS}_i \equiv 2 \times [\ln \mathcal{L}_i(\mathbf{d}|\hat{A}) - \ln \mathcal{L}_i(\mathbf{d}|0)]$, for $\hat{A} > 0$, and $\mathrm{TS}_i = 0$ if $\hat{A} < 0$.

We additionally analyze the stacked but uncalibrated off spectra. This is valuable because the off data are subtracted and divided from the on data to remove the instrumental baselines, but this may cause features in the off spectra to be imprinted on the calibrated flux densities. Therefore, statistically significant excesses that appear in both the calibrated source flux density spectra and the off system temperatures can be vetoed, as they are inconsistent with, or at least do not require, an axion interpretation. In our analysis, we veto any excess in the calibrated on data which appears with a 97.5th percentile discovery TS in the off data. Note that we determine the TS percentiles by using the full distribution of observed TSs.

The 95% upper limits on the flux densities, defined relative to the single-channel frequency bin widths δf_{fid} given in Table I, are shown in Fig. 1. We compare the upper limits to the expected limits from the ideal radiometer equation, which assumes that all of the noise is thermal at the system temperature. The true limits are slightly weaker likely because of sources of systematic uncertainty,

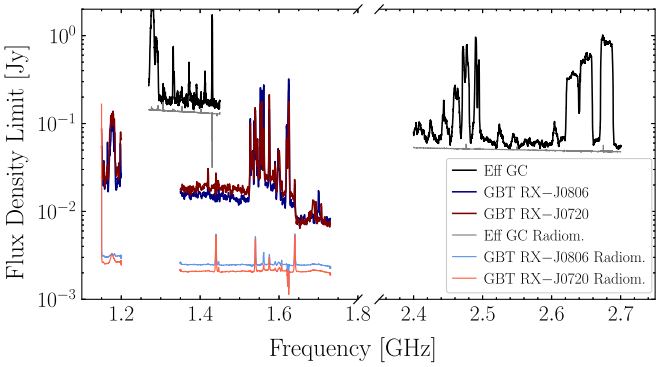

FIG. 1. The 95% upper limits on the signal flux for the indicated sources from the GBT and Effelsberg observations. These upper limits apply to monochromatic signals at the widths δf_{fid} given in Table I. These curves have been down-sampled for visualization purposes. We compare these limits with the 95% upper limits expected from the ideal radiometer equation under the assumption that the only source of statistical uncertainty is thermal noise at the total system temperature.

such as uncertainties in the background model and instrumental uncertainties not fully captured by the calibration procedure.

We search for evidence of an axion signal by using the discovery TSs. We apply a discovery threshold of TS > 100, which was defined before performing the analysis and not modified afterward. From Monte Carlo (MC) simulations of the null hypothesis, we find that this TS threshold corresponds to approximately 5σ local significance (see Supplemental Material [24] for details). After applying the analysis procedure described above, we find no axion signal candidates at or beyond the detection significance in any of the observations, and the distributions of observed TSs are consistent with the null hypothesis. Note that HI emission frequencies are excluded automatically in our analysis by the off veto criterion.

Results.—To translate the flux-density limits from Fig. 1 into limits on the axion-photon coupling, we closely follow the theoretical modeling presented in Refs. [3,4] for computing the axion-induced radio fluxes from these specific sources.

The radiated power for a single INS depends on $g_{a\gamma\gamma}$, the polar magnetic field strength B_0 (assuming a dipole field configuration), the NS mass (which we fix at 1 $M_\odot$, since this value does not significantly affect the flux), the NS spin period P, the axion mass m_a, the DM density ρ_∞ in the neighborhood of the NS but asymptotically far away from its gravitational potential, and the velocity dispersion v_0 of the ambient DM. For the local INSs, we take $v_0 = 200$ km/s and $\rho_\infty = 0.4$ GeV/ cm^3 [42–44]. For the GC analysis, we assume the DM follows an Navarro-Frenk-White (NFW) [45,46] density profile near the GC, normalized to give the local DM density above and with a scale radius of 20 kpc (see, e.g., [4]). For RX J0806.4-4123 we take $\log_{10}(B_0/G) = 13.40$ and $P = 11.4$ s while for RX J0720.4-3125 we use $\log_{10}(B_0/G) = 13.53$ and $P = 8.4$ s. We note that these parameters were inferred from spin-down measurements performed in the x-ray band [47–49]. We take RX J0806.4-4123 and RX J0720.4-3125 to be at distances of 250 and 360 pc from Earth, respectively [48].

Given these parameters, we estimate the radiated power following Refs. [3,6]. However, we note that a fully self-consistent calculation of the axion-induced radiation has yet to be performed. Reference [6] corrected the assumption in Ref. [3] that the axions travel along radial trajectories, but Ref. [6] did not account for the fact that the outgoing radiation is strongly refracted in the inhomogeneous magnetosphere, as we point out in Supplemental Material [24]. As a dedicated simulation of the axion-induced radiation is beyond the scope of this work, we estimate the power with the following approximation. We assume (i) that all axions travel along radial trajectories, as in Ref. [3], (ii) that all NSs are aligned rotators (magnetically misaligned rotators give nearly identical results [3]), and (iii) that the magnetosphere is well described by the Goldreich-Julian (GJ) model [50]. Then, following Ref. [3], we compute the angular power distribution $dP/d\theta$ of radio emission as a function of the angle from the polar axis θ. However, we assign to each NS a single power value equal to $\int (dP/d\theta) d\theta$, and we assume that the flux is radiated from each NS isotropically. With the latter assumption, we find results are consistent with those in Ref. [6], which correctly accounted for the isotropic axion phase space. For example, taking NS parameters describing the nearby isolated NSs studied in this work (and assuming aligned rotators), the formalism in Ref. [6] predicts fluxes $\sim$50% larger than inferred by our simpler calculation. We chose this simpler formalism, however, because it is likely that the more complicated computation in Ref. [6] must be modified due to the refraction of outgoing radio photons, which could result in an anisotropic signal [though from the studies in Ref. [6] we do not expect such calculations to change the flux predictions by more than an $\mathcal{O}(1)$ amount]. Given an improved theoretical predictions in the future, our results may be reinterpreted using the supplemental data [51].

In Ref. [4], it is shown that more complicated magnetosphere models, such as the electrosphere model, give similar results. In particular, the total radiated power averaged over NS populations differed by $\sim$20% between the electrosphere and GJ models in Ref. [4]. Active pulsars and magnetars could have magnetospheres which deviate more substantially from the GJ model by having large charge-pair multiplicities, though this is expected to affect only a small fraction of the NSs within the populations and to not affect the nearby isolated NSs studied in this work (see [4] and references therein).

The width of the signal in frequency space is determined in part by the asymptotic energy dispersion of the DM, which is set by v_0. This induces a $\delta f/f \lesssim 10^{-6}$ contribution to the width from the INSs. However, as discussed more in Supplemental Material [24] and in Ref. [5], the signals are Doppler broadened when refracting or reflecting from the rotating plasma, inducing a frequency broadening closer to $\delta f/f \sim 5 \times 10^{-6}$ and justifying the bin widths taken in Table I.

Since we do not actually know which specific NSs are being targeted in the Effelsberg GC analysis (and similarly in the GBT population analyses discussed in Supplemental Material [24]), we model the population of NSs (number density, spatial distribution, magnetic field, and spin period) within the GC region as a whole, closely following Ref. [4]. In particular, two models for the NS magnetic field and period distributions were developed in that work, based on fits to existing pulsar data. We conservatively choose the model which yields weaker constraints as our fiducial model. In practice, our fiducial NS population model (model II in Ref. [4]) assumes that magnetic fields quickly decay after the NSs cross the pulsar death line, while the optimistic model (model I in Ref. [4]) assumes that the

magnetic fields decay more slowly. We also follow Ref. [4] when modeling the spatial distribution of NSs within the Galactic bulge and disk. For the Effelsberg analysis, we perform $\mathcal{O}(10^3)$ MC simulations of the NS population model and profile over the simulation results when calculating the expected flux and associated 95% limit.

Given the fiducial models we have described, we obtain the limits on $g_{a\gamma\gamma}$ shown in Fig. 2. The orange band represents the predicted $g_{a\gamma\gamma}$ for the QCD axion, and the gray shaded regions represent existing constraints from other experiments. We obtain limits that are stronger than those from CAST [52] and comparable to constraints from the UF [18] and RBF [16,17] haloscopes, while the *S*-band Effelsberg constraints exclude previously unexplored parameter space. The green shaded band in Fig. 2 represents two dominant sources of uncertainty for the GC analysis. The top of the band is derived by assuming that the DM profile follows a cored density profile with a core radius of 0.6 kpc; this radius is chosen based on recent hydrodynamic simulations which suggest that the DM density may be modified in the inner ∼0.6 kpc where the baryons dominate the gravitational potential, though these same simulations suggest an enhancement of the central DM density may also be possible [53]. The lower boundary of the band assumes the fiducial NFW DM profile but takes the alternate NS population model (model I) from Ref. [4].

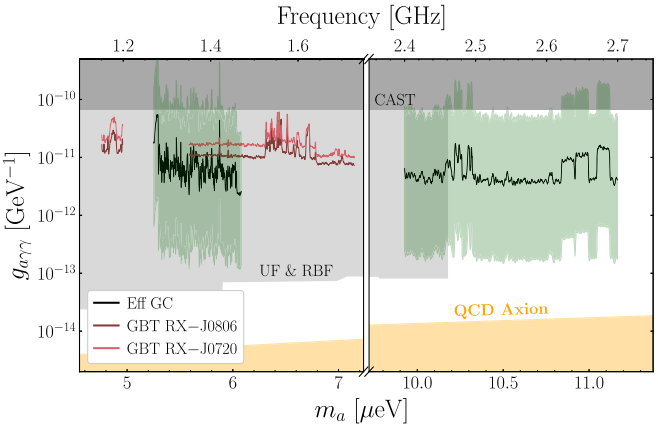

FIG. 2. The one-sided 95% upper limits on $g_{a\gamma\gamma}$ as a function of the axion mass m_a from this work are shown as colored lines (GBT INS observations) and black lines (Effelsberg GC observations). Previous limits from the CAST helioscope and the UF and RBF haloscopes are shown in shaded gray. The range of couplings expected for the QCD axion is shaded in orange. Note that the fiducial GC limits assume an NFW DM profile and the conservative NS population model (model II) from Ref. [4]. The green band depicts theoretical uncertainties on the $g_{a\gamma\gamma}$ limit associated with the GC analysis for the Effelsberg data. The top of the band assumes an NFW DM density profile with a 0.6 kpc core, while the bottom of the band uses the alternate NS population model in Ref. [4] (model I).

Discussion.—In this work, we performed the first dedicated radio telescope search for signatures of axion DM from axion-photon conversion in NS magnetospheres. We found no evidence for axion DM and set some of the strongest constraints to date on the axion DM scenario. These results show that radio searches for axion DM are a promising path forward, analogous to indirect detection for WIMP DM searches, which should proceed in parallel with laboratory experiments for discovering or excluding axion DM. Additional flux sensitivity is needed in order to reach the QCD axion band at the frequencies targeted in this work. This sensitivity may be available with the upcoming Square Kilometer Array-mid [54] or may already be achievable with the FAST radio telescope [55], since at constant system temperature the sensitivity to $g_{a\gamma\gamma}$ scales inversely with the square root of the effective area [4].

Our work strongly motivates searching with the GBT or Effelsberg radio telescope for evidence of axion DM at higher frequencies, closer to 6 GHz, to probe the axion mass window around $m_a \approx 25$ μeV. There is mounting evidence that points toward 25 μeV as a likely mass for the axion [56,57], and the axion-photon coupling may also be enhanced [58] and, thus, within reach of GBT and Effelsberg searches. This work also motivates additional effort in modeling the population evolution of NS magnetic fields and spin periods, as these are the largest sources of uncertainty in our population analyses, as well as further efforts to understand the distribution of DM in the inner Galaxy. More work on the axion-induced signal itself from individual INSs would be also useful, as a full calculation of the axion-induced radio signal does not yet exist; such results could lead to reinterpretations of the limits presented in this Letter using supplemental data [51].

The Green Bank Observatory is a facility of the National Science Foundation operated under cooperative agreement by Associated Universities, Inc. This work was based on observations with the 100 m telescope of the Max-Planck-Institut für Radioastronomie at Effelsberg. We thank Amber Bonsall for assistance with GBT data taking and Anson Hook for collaboration in the early stages of this work. We also thank Karl Van Bibber, Christopher Dessert, Gregory Desvignes, Tom Edwards, Reyco Henning, Jonathan Ouellet, Nicholas Rodd, Katelin Schutz, Chenoa Tremblay, Mauro Valli, and Kathryn Zurek for helpful comments and discussions. This work was supported in part by the DOE Early Career Grant No. DESC0019225 and through computational resources and services provided by Advanced Research Computing at the University of Michigan, Ann Arbor. J. W. F. was supported in part by the Munich Institute for Astro- and Particle Physics (MIAPP) which is funded by the Deutsche Forschungsgemeinschaft (DFG, German Research Foundation) under Germany's Excellence Strategy—EXC-2094-390783311. O. M. acknowledges support by JSPS KAKENHI Grants No. JP17H04836,

No. JP18H04340, and No. JP18H04578 and by World Premier International Research Center Initiative (WPI Initiative), MEXT, Japan. R. P. E. acknowledges financial support by the European Research Council for the ERC Synergy Grant BlackHoleCam under Contract No. 610058. Basic research in radio astronomy at the Naval Research Laboratory is supported by 6.1 base funding.

Digitized versions of main figures along with raw and processed data products may be found in supplemental data [51].

*fosterjw@umich.edu
†C.Weniger@uva.nl
‡bsafdi@umich.edu

[1] M. S. Pshirkov, Conversion of Dark matter axions to photons in magnetospheres of neutron stars, J. Exp. Theor. Phys. **108**, 384 (2009).
[2] F. P. Huang, K. Kadota, T. Sekiguchi, and H. Tashiro, Radio telescope search for the resonant conversion of cold dark matter axions from the magnetized astrophysical sources, Phys. Rev. D **97**, 123001 (2018).
[3] A. Hook, Y. Kahn, B. R. Safdi, and Z. Sun, Radio Signals from Axion Dark Matter Conversion in Neutron Star Magnetospheres, Phys. Rev. Lett. **121**, 241102 (2018).
[4] B. R. Safdi, Z. Sun, and A. Y. Chen, Detecting axion dark matter with radio lines from neutron star populations, Phys. Rev. D **99**, 123021 (2019).
[5] R. A. Battye, B. Garbrecht, J. I. McDonald, F. Pace, and S. Srinivasan, Dark matter axion detection in the radio/mm-waveband, Phys. Rev. D **102**, 023504 (2020).
[6] M. Leroy, M. Chianese, T. D. P. Edwards, and C. Weniger, Radio signal of axion photon conversion in neutron stars: A ray tracing analysis, Phys. Rev. D **101**, 123003 (2020).
[7] J. Preskill, M. B. Wise, and F. Wilczek, Cosmology of the invisible axion, Phys. Lett. **120B**, 127 (1983).
[8] L. F. Abbott and P. Sikivie, A cosmological bound on the invisible axion, Phys. Lett. **120B**, 133 (1983).
[9] M. Dine and W. Fischler, The not so harmless axion, Phys. Lett. **120B**, 137 (1983).
[10] R. D. Peccei and H. R. Quinn, Constraints imposed by *CP* conservation in the presence of instantons, Phys. Rev. D **16**, 1791 (1977).
[11] R. D. Peccei and H. R. Quinn, *CP* Conservation in the Presence of Instantons, Phys. Rev. Lett. **38**, 1440 (1977).
[12] S. Weinberg, A New Light Boson?, Phys. Rev. Lett. **40**, 223 (1978).
[13] F. Wilczek, Problem of Strong *P* and *T* Invariance in the Presence of Instantons, Phys. Rev. Lett. **40**, 279 (1978).
[14] I. G. Irastorza and J. Redondo, New experimental approaches in the search for axion-like particles, Prog. Part. Nucl. Phys. **102**, 89 (2018).
[15] J. Beringer *et al.* (Particle Data Group), Review of particle physics (RPP), Phys. Rev. D **86**, 010001 (2012).
[16] S. De Panfilis, A. C. Melissinos, B. E. Moskowitz, J. T. Rogers, Y. K. Semertzidis, W. U. Wuensch, H. J. Halama, A. G. Prodell, W. B. Fowler, and F. A. Nezrick, Limits on the Abundance and Coupling of Cosmic Axions at $4.5 < m(a) < 5.0$ μev, Phys. Rev. Lett. **59**, 839 (1987).
[17] W. U. Wuensch, S. De Panfilis-Wuensch, Y. K. Semertzidis, J. T. Rogers, A. C. Melissinos, H. J. Halama, B. E. Moskowitz, A. G. Prodell, W. B. Fowler, and F. A. Nezrick, Results of a laboratory search for cosmic axions and other weakly coupled light particles, Phys. Rev. D **40**, 3153 (1989).
[18] C. Hagmann, P. Sikivie, N. S. Sullivan, and D. B. Tanner, Results from a search for cosmic axions, Phys. Rev. D **42**, 1297 (1990).
[19] S. J. Asztalos, G. Carosi, C. Hagmann, D. Kinion, K. van Bibber, M. Hotz, L. J. Rosenberg, G. Rybka, J. Hoskins, J. Hwang, P. Sikivie, D. B. Tanner, R. Bradley, and J. Clarke, SQUID-Based Microwave Cavity Search for Dark-Matter Axions, Phys. Rev. Lett. **104**, 041301 (2010).
[20] N. Du, N. Force, R. Khatiwada, E. Lentz, R. Ottens *et al.* (ADMX Collaboration), A Search for Invisible Axion Dark Matter with the Axion Dark Matter Experiment, Phys. Rev. Lett. **120**, 151301 (2018).
[21] T. Braine, R. Cervantes, N. Crisosto, N. Du, S. Kimes *et al.* (ADMX Collaboration), Extended Search for the Invisible Axion with the Axion Dark Matter Experiment, Phys. Rev. Lett. **124**, 101303 (2020).
[22] B. M. Brubaker, L. Zhong, S. K. Lamoreaux, K. W. Lehnert, and K. A. van Bibber, HAYSTAC axion search analysis procedure, Phys. Rev. D **96**, 123008 (2017).
[23] R. M. Prestage, M. Bloss, J. Brandt, H. Chen, R. Creager, P. Demorest, J. Ford, G. Jones, A. Kepley, A. Kobelski, P. Marganian, M. Mello, D. McMahon, R. McCullough, J. Ray, D. Anish Roshi, D. Werthimer, and M. Whitehead, The versatile GBT astronomical spectrometer (VEGAS): Current status and future plans, in *Proceedings of the 2015 URSI-USNC Radio Science Meeting* (IEEE, Vancouver, 2015) p. 4.
[24] See Supplemental Material at http://link.aps.org/supplemental/10.1103/PhysRevLett.125.171301 for additional results and explanations of our methods that clarify and support the results presented in the main Letter, which includes Refs. [25–35].
[25] R. A. Perley and B. J. Butler, Integrated polarization properties of 3C48, 3C138, 3C147, and 3C286, Astrophys. J. Suppl. Ser. **206**, 16 (2013).
[26] R. A. Perley and B. J. Butler, An accurate flux density scale from 50 MHz to 50 GHz, Astrophys. J. Suppl. Ser. **230**, 7 (2017).
[27] A. W. Hotan, W. van Straten, and R. N. Manchester, PSRCHIVE and PSRFITS: An open approach to radio pulsar data storage and analysis, Pub. Astron. Soc. Aust. **21**, 302 (2004).
[28] R. M. Crocker, D. I. Jones, F. Aharonian, C. J. Law, F. Melia, T. Oka, and J. Ott, Wild at heart: The particle astrophysics of the Galactic Centre, Mon. Not. R. Astron. Soc. **413**, 763 (2011).
[29] W. Reich, P. Reich, and E. Fuerst, The Effelsberg 21 CM radio continuum survey of the Galactic plane between L = 357 deg. and L= 95.5 deg., Astron. Astrophys. Suppl. Ser. **83**, 539 (1990), https://ui.adsabs.harvard.edu/abs/1990A%26AS...83..539R/abstract.

[30] S. S. Wilks, The large-sample distribution of the likelihood ratio for testing composite hypotheses, Ann. Math. Stat. **9**, 60 (1938).
[31] M. Gray, Maser molecules, in *Maser Sources in Astrophysics, Cambridge Astrophysics* (Cambridge University Press, Cambridge, England, 2012), pp. 156–185.
[32] R. P. Norris and R. S. Booth, Observations of OH masers in W3 OH., Mon. Not. R. Astron. Soc. **195**, 213 (1981).
[33] H. Qiao, J. Li, Z. Shen, X. Chen, and X. Zheng, The catalogues and mid-infrared environment of interstellar OH masers, Mon. Not. R. Astron. Soc. **441**, 3137 (2014).
[34] J. L. Caswell, Positions of hydroxyl masers at 1665 and 1667 MHz, Mon. Not. R. Astron. Soc. **297**, 215 (1998).
[35] M. McCall and D. Censor, Relativity and mathematical tools: Waves in moving media, Am. J. Phys. **75**, 1134 (2007).
[36] P. Lazarus, R. Karuppusamy, E. Graikou, R. N. Caballero, D. J. Champion, K. J. Lee, J. P. W. Verbiest, and M. Kramer, Prospects for high-precision pulsar timing with the new Effelsberg PSRIX backend, Mon. Not. R. Astron. Soc. **458**, 868 (2016).
[37] B. Garwood, P. Marganian, J. Braatz, and R. Maddalena, GBTIDL data analysis software, http://gbtidl.nrao.edu/ (2005).
[38] http://dspsr.sourceforge.net.
[39] W. van Straten and M. Bailes, DSPSR: Digital signal processing software for pulsar astronomy, Pub. Astron. Soc. Aust. **28**, 1 (2011).
[40] G. Cowan, K. Cranmer, E. Gross, and O. Vitells, Asymptotic formulae for likelihood-based tests of new physics, Eur. Phys. J. C **71**, 1554 (2011); Erratum, Eur. Phys. J. C **73**, 2501 (2013).
[41] G. Cowan, K. Cranmer, E. Gross, and Ofer Vitells, Power-constrained limits, arXiv:1105.3166.
[42] J. Bovy and S. Tremaine, On the local dark matter density, Astrophys. J. **756**, 89 (2012).
[43] J. I. Read, The local dark matter density, J. Phys. G **41**, 063101 (2014).
[44] K. Schutz, T. Lin, B. R. Safdi, and C.-L. Wu, Constraining a Thin Dark Matter Disk with Gaia, Phys. Rev. Lett. **121**, 081101 (2018).
[45] J. F. Navarro, C. S. Frenk, and S. D. M. White, The Structure of cold dark matter halos, Astrophys. J. **462**, 563 (1996).
[46] J. F. Navarro, C. S. Frenk, and S. D. M. White, A Universal density profile from hierarchical clustering, Astrophys. J. **490**, 493 (1997).
[47] D. L. Kaplan and M. H. van Kerkwijk, A coherent timing solution for the nearby isolated neutron star RX J0720.4-3125, Astrophys. J. **628**, L45 (2005).
[48] D. L. Kaplan and M. H. van Kerkwijk, Constraining the spin-down of the nearby isolated neutron star RX J0806.4-4123, and implications for the population of nearby neutron stars, Astrophys. J. **705**, 798 (2009).
[49] M. Buschmann, R. T. Co, C. Dessert, and B. R. Safdi, X-ray search for axions from nearby isolated neutron stars, arXiv:1910.04164.
[50] P. Goldreich and W. H. Julian, Pulsar electrodynamics, Astrophys. J. **157**, 869 (1969).
[51] J. Foster *et al.*, https://doi.org/10.5281/zenodo.4058674.
[52] V. Anastassopoulos *et al.* (CAST Collaboration), New CAST limit on the axion-photon interaction, Nat. Phys. **13**, 584 (2017).
[53] P. F. Hopkins *et al.*, FIRE-2 simulations: Physics versus numerics in galaxy formation, Mon. Not. R. Astron. Soc. **480**, 800 (2018).
[54] A. Weltman *et al.*, Fundamental physics with the square kilometre array, Pub. Astron. Soc. Aust. **37**, e002 (2020).
[55] R. Nan, D. Li, C. Jin, Q. Wang, L. Zhu, W. Zhu, H. Zhang, Y. Yue, and L. Qian, The five-hundred aperture spherical radio telescope (fast) project, Int. J. Mod. Phys. D **20**, 989 (2011).
[56] M. Buschmann, J. W. Foster, and B. R. Safdi, Early-Universe Simulations of the Cosmological Axion, Phys. Rev. Lett. **124**, 161103 (2020).
[57] V. B. Klaer and G. D. Moore, The dark-matter axion mass, J. Cosmol. Astropart. Phys. 11 (2017) 049.
[58] P. Agrawal, J. J. Fan, M. Reece, and L.-T. Wang, Experimental targets for photon couplings of the QCD axion, J. High Energy Phys. 02 (2018) 006.